Simultaneous determination of effective spin-orbit torque fields in magnetic structures with in-plane anisotropy

Luo, Feilong; Goolaup, Sarjoosing; Law, Wai Cheung; Li, Sihua; Tan, Funan; Engel, Christian; Zhou, Tiejun; Lew, Wen Siang

2017

Luo, F., Goolaup, S., Law, W. C., Li, S., Tan, F., Engel, C., . . . Lew, W. S. (2017). Simultaneous determination of effective spin-orbit torque fields in magnetic structures with in-plane anisotropy. Physical Review B, 95(17), 174415-. doi:10.1103/PhysRevB.95.174415

https://hdl.handle.net/10356/81139

https://doi.org/10.1103/PhysRevB.95.174415

Simultaneous determination of effective spin-orbit torque fields in magnetic structures with in-plane anisotropy

Feilong Luo,[1,2] Sarjoosing Goolaup,[1] Wai Cheung Law,[1] Sihua Li,[1] Funan Tan,[1] Christian Engel,[1] Tiejun Zhou,[2] and Wen Siang Lew[1,*]

[1]*School of Physical and Mathematical Sciences, Nanyang Technological University, 21 Nanyang Link, Singapore 637371*

[2]*Data Storage Institute, 2 Fusionopolis Way, #08-01 Innovis, Singapore 138634*

(Received 27 January 2017; revised manuscript received 5 April 2017; published 10 May 2017)

The strength of spin-orbit torque in ferromagnetic structures is characterized by fieldlike and dampinglike effective fields. Conventionally, two distinct measurement approaches are employed to quantify the magnitude of the respective effective fields in structures with in-plane magnetic anisotropy. Here, we propose and demonstrate a self-validating method, which enables simultaneous quantification of both the fieldlike and dampinglike terms in structures with in-plane magnetic anisotropy. An analytical expression is derived and validated by harmonic Hall resistance measurement. Both the fieldlike and dampinglike effective fields are extracted from a single measurement using the derived fitting functions for the second harmonic Hall resistance. The first harmonic Hall resistance acts as a reference to confirm that the experimental parameters are consistent with the derived equations.

DOI: 10.1103/PhysRevB.95.174415

I. INTRODUCTION

Spin accumulation at the interface of nonmagnetic heavy metals (HM)/ferromagnetic material (FM) influences the magnetization of the adjacent FM layer *via* the spin-orbit torque (SOT) [1]. The two main phenomena contributing to the spin accumulation are the bulk spin Hall effect arising from spin scattering in the HM layer and, Rashba effect, which is an interfacial spin-orbit coupling at the FM/HM interface [2–10]. In the FM layer, the exchange interaction between the spin accumulation and local magnetic moment induces the SOT, which comprises of the fieldlike torque $\boldsymbol{\tau}_F = -H_F \mathbf{M}_s \times \mathbf{s}$ and the dampinglike torque $\boldsymbol{\tau}_D = -H_D \mathbf{M}_s \times (\mathbf{m} \times \mathbf{s})$, where $\mathbf{s}$ is the unit vector of the spin of the electrons diffusing into the FM layer, $\mathbf{M}_s$ is the saturation magnetization of the FM layer, and $\mathbf{m}$ is the unit vector of $\mathbf{M}_s$ [1,10–14]. As such, the intensities of the torques are generally characterized by the two corresponding effective fields: fieldlike term $\mathbf{H}_F = H_F \mathbf{s}$ and dampinglike term $\mathbf{H}_D = H_D \mathbf{m} \times \mathbf{s}$ [6,8,10,12,15–20].

Significant efforts have been devoted to characterizing the SOT effective fields in ferromagnetic heterostructures consisting of ultrathin FM layer with strong perpendicular magnetic anisotropy (PMA), sandwiched between a nonmagnetic HM and/or an oxide layer [8,15,18,19,21–27]. A number of measurement methods can be used to quantify the respective effective fields, such as, current-induced domain wall motion [8,21,28–30], ferromagnetic resonance (FMR) techniques [31–38], and SOT-assisted magnetization switching [6,20,22,35,39]. However, the measured amplitude of SOT effective field depends on the method used for quantification [8,17,25,31–33,36,40,41], based on the linear relationship between the spin Hall angle and the SOT effective field [9,17,42,43]. The most widely used measurement technique for SOT effective fields characterization is the harmonic Hall measurement [18,19,23,29,44]. In this technique, the fieldlike and dampinglike terms are extracted from the harmonic Hall voltages with respect to externally applied magnetic fields along transverse and longitudinal directions of electric current, respectively.

The investigation of SOT in magnetic heterostructures with in-plane magnetic anisotropy (IMA) has been gaining more interest recently, as the SOT-induced switching scheme, where the magnetic easy axis is in-plane and collinear with the applied current, is in particular promising for applications in three-terminal SOT devices [43]. Additionally, the IMA systems are being used as a platform to characterize the SOT in topological insulator structures, where large spin Hall angles have been obtained [45–47]. Unlike in PMA systems, the corresponding torque in IMA systems acts in both in-plane and out-of-plane orientations, making characterization of the effective fields difficult. As such, the most common method for characterizing the SOT in IMA systems is *via* the FMR technique, which provides the spin Hall angle, the ratio of spin-polarized current to charge current [37,38]. However, in the FMR technique, the measured SOT effective fields are highly dependent on the geometry of the device under test [34]. For quantitative characterization of the SOT effective fields, Hayashi *et al.* proposed a low frequency harmonic measurement method [20]. Using two distinct measurements, the fieldlike and dampinglike SOT effective fields in ferromagnetic materials can be obtained. The fieldlike term is measured through sweeping a small externally applied magnetic field along the easy axis of the magnetic wire, while the dampinglike term is measured through anisotropy magnetoresistance (AMR) effect. Alternatively, the two SOT effective fields can be obtained through sweeping a magnetic field along the direction normal to the IMA film. The fieldlike term is obtained in a low-field regime whereas the dampinglike term is computed in a high-field regime sweep. However, such measurement configurations may result in different values for the two terms and that may lead to inconsistency during characterization. Moreover, this technique is based on the assumption of a uniform magnetization configuration. Any

*Corresponding author: wensiang@ntu.edu.sg

deviation in the magnetization while the external magnetic field is swept will corrupt the signal and result in the subsequent calculations to be erroneous. In polycrystalline magnetic films, the value of the magnetization will vary as the external magnetic field is swept [48]. For external fields lower than the saturation field, magnetic moments within crystal grains may be orientated in different directions due to the crystalline magnetic anisotropy [48]. As such, the measurement of effective SOT fields in polycrystalline films may lead to inaccurate results.

In this work, we have developed and experimentally tested a harmonic Hall technique, where a single measurement can concurrently provide quantitative information on both the fieldlike and dampinglike SOT terms in IMA structures. This technique enables the results to be insulated from measurement artefacts. Starting from the standard total energy of a magnetic system, the equations to compute the corresponding SOT effective fields are derived. By fitting the measured second harmonic Hall resistance with our derived equation, the fieldlike and dampinglike terms can be extracted. The first harmonic Hall resistance verifies the rotation of magnetization and is used to obtain the parameters in the derived equations. In this method, a constant longitudinal magnetic field is applied along the wire direction to ensure a uniform magnetization along the long axis of the wire. A transverse sweeping magnetic field is applied and the second harmonic Hall resistance with respect to the cosine of the azimuthal angle of the magnetic moment is measured. Experimental verification was carried out in stacks comprising of Ta/Co/Pt with IMA. The Ta thickness dependence of the SOT effective fields in the Ta/Co/Pt stack is investigated. For a film stack of Ta(10 nm)/Co(2 nm)/Pt(5 nm) with IMA, the fieldlike term is found to be ∼9 Oe per 10^{11} Am^{-2} and the dampinglike term is ∼80 Oe per 10^{11} Am^{-2}.

II. ANALYTICAL DERIVATION

This section describes how the analytical formulas are obtained. The derivation starts from the magnetic energy expression E of a magnetic system with IMA, which is used to obtain the relationship between the magnetization angles φ, θ and magnetic fields $H_{(x,y,z)}$. The modulation of the magnetization angle induced by SOT fields is then introduced, and converted into measurable changes of harmonic Hall resistance. The terms for calculating SOT fields are obtained through fitting second harmonic Hall resistance with respect to the cosine of the azimuthal angle of magnetization, instead of the widely used transverse sweeping field.

For a magnetic wire system with IMA, as depicted in Fig. 1(a), the magnetic energy E is given by

$$E = \left(N_z M_s^2 - K_\perp\right)\sin^2\theta - M_s H_z \sin\theta - M_s H_x \cos\theta\cos\varphi - M_s H_y \cos\theta \sin\varphi, \quad (1)$$

where N_z is the demagnetizing factor along z direction and $K_\perp$ is the interface perpendicular magnetic anisotropy energy density which may be present in ultrathin films [49]. M_s is the saturation magnetization of the wire, $H_{(x,y,z)}$ are the effective magnetic fields along the three basic vector directions, inclusive of the externally applied magnetic fields

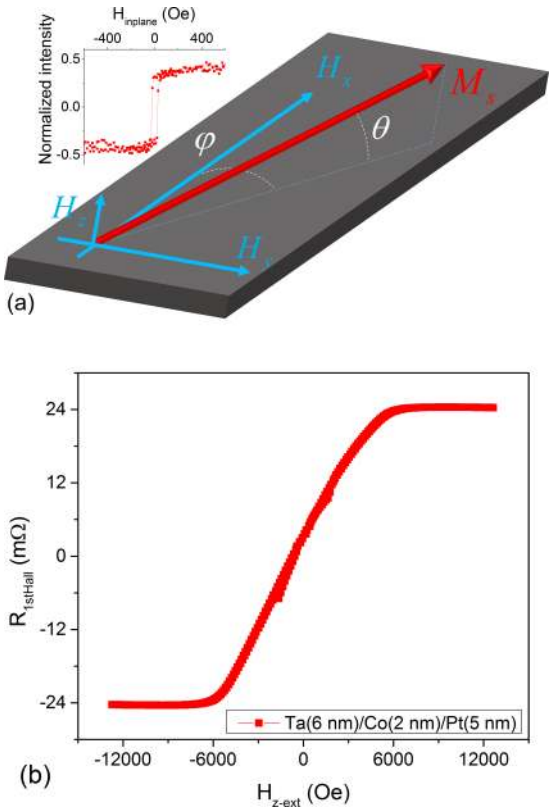

FIG. 1. (a) Orientation of magnetization under magnetic fields. Inset is the normalized longitudinal MOKE measurement for Ta(6 nm)/Co(2 nm)/Pt(5 nm) stack. (b) Hall resistances with respect to applied out-of-plane field for patterned Hall cross with the stack. Measurements indicate in-plane magnetic anisotropy property in the investigated stacks.

$[H_{(x\text{-ext},y\text{-ext},z\text{-ext})}]$ and the SOT fields (H_F and H_D). φ and θ are the azimuthal and polar angles of $\mathbf{M}_s$. The first term in Eq. (1) represents the in-plane magnetic anisotropy energy of the magnetic wire, which is positive. The three terms with the field components are the Zeeman energy of the wire. For derivation simplicity, the expression $2(N_z M_s^2 - K_\perp)$ is written as $M_s H_\perp$, where $H_\perp$ represents the effective field that align the magnetization along the in-plane orientation. To obtain the relationship between the magnetization angles and magnetic fields $H_{(x,y,z)}$, partial derivatives of Eq. (1) with respect to the variables φ and θ are carried out,

$$\frac{\partial E}{\partial \theta} = M_s H_\perp \sin\theta\cos\theta - M_s H_z \cos\theta + M_s H_x \sin\theta\cos\varphi + M_s H_y \sin\theta\sin\varphi = 0, \quad (2)$$

$$\frac{\partial E}{\partial \varphi} = M_s H_x \cos\theta\sin\varphi - M_s H_y \cos\theta\cos\varphi = 0. \quad (3)$$

In order to simplify Eqs. (2) and (3), θ is assumed to be very small which results in $\cos\theta \approx 1$. Equations (2) and (3) are solved to obtain the equilibrium angles of φ and θ, $\sin\theta = \frac{H_z}{H_\perp + H_x\cos\varphi + H_y\sin\varphi}$ and $\tan\varphi = \frac{H_y}{H_x}$. In the regime where $H_\perp \gg H_{(x,y)}$, the term $H_x\cos\varphi + H_y\sin\varphi$ in the expression of $\sin\theta$ can be ignored. The stable angles, φ_0 and θ_0, can be determined

by the externally applied fields $H_{(x\text{-ext},y\text{-ext},z\text{-ext})}$ as

$$\sin\theta_0 = \frac{H_{z\text{-ext}}}{H_\perp}, \tag{4}$$

$$\tan\varphi_0 = \frac{H_{y\text{-ext}}}{H_{x\text{-ext}}}. \tag{5}$$

For IMA system, the SOT effective fields are given by: fieldlike term $\mathbf{H}_F = H_F\mathbf{y}$ and dampinglike term $\mathbf{H}_D = H_D\mathbf{m}\times\mathbf{y}$, where $\mathbf{m}$ is along in-plane direction and $\mathbf{y}$ is the in-plane unit vector pointing towards transverse to charge current direction [20]. When an alternating electric current (ac) with a low frequency ω, $I = I_0\sin\omega t$, is applied in the wire, the synchronous fieldlike term is $\mathbf{H}_F = (H_F\sin\omega t)\mathbf{y}$. The dampinglike term is $\mathbf{H}_D = (H_D\sin\omega t)\cos\varphi_0\mathbf{z}$, where $\cos\varphi_0\mathbf{z}$ arises from the expression $\mathbf{m}\times\mathbf{y}$. Due to the SOT effective fields, small modulations in the magnetization from the stable angles are induced, $\Delta\theta_0$ and $\Delta\varphi_0$. The modulations can be estimated through a partial derivative of Eqs. (4) and (5) with respect to φ_0 and θ_0, $\Delta\theta_0 \approx \Delta\sin\theta_0 \approx \frac{1}{H_\perp}\Delta H_{z\text{-ext}}$, $\Delta\tan\varphi_0 = \frac{\Delta\varphi_0}{\cos^2\varphi_0} = \frac{1}{H_{x\text{-ext}}}\Delta H_{y\text{-ext}}$. As the effective fields H_D and H_F act along the z and y axes, respectively, $\Delta H_{z\text{-ext}}$ and $\Delta H_{y\text{-ext}}$ can be replaced with H_D and H_F. The modulations of magnetization angle induced by SOT effective fields is then given as

$$\Delta\theta_0 = \frac{1}{H_\perp}H_D\cos\varphi_0\sin\omega t, \tag{6}$$

$$\Delta\varphi_0 = \frac{\cos^2\varphi_0}{H_{x\text{-ext}}}H_F\sin\omega t. \tag{7}$$

From the above discussion, the tilt angle of the magnetization with respect to the easy axis is determined by the externally applied fields and SOT effective fields, $\theta = \theta_0 + \Delta\theta_0$ and $\varphi = \varphi_0 + \Delta\varphi_0$.

The modulations of the magnetization angle are reflected as measurable changes in the harmonic Hall resistance. The total Hall resistance R_{Hall} of the wire consists of two components: anomalous Hall effect (AHE) resistance, $R_{\text{A}} = R_{\text{AHE}}\sin\theta$, and planar Hall effect (PHE) resistance, $R_{\text{P}} = R_{\text{PHE}}\cos^2\theta\sin 2\varphi$, where R_{AHE} and R_{PHE} are the amplitudes of AHE and PHE resistances, respectively [7,12,50,51]. In the presence of an ac current, the Hall voltage is given by $V_{\text{Hall}} = R_{\text{AHE}}I_0\sin\theta\sin\omega t + R_{\text{PHE}}I_0\cos^2\theta\sin 2\varphi\sin\omega t$. Substituting θ and φ with $\theta_0 + \Delta\theta_0$ and $\varphi_0 + \Delta\varphi_0$, respectively, into the expression of V_{Hall} gives

$$\frac{V_{\text{Hall}}}{I_0} = R_{\text{Hall}} = R_{\text{AHE}}\sin(\theta_0+\Delta\theta_0)\sin\omega t + R_{\text{PHE}}\cos^2(\theta_0+\Delta\theta_0)\sin[2(\varphi_0+\Delta\varphi_0)]\sin\omega t. \tag{8}$$

From Eq. (8), the SOT induced magnetization modulations, $\Delta\theta_0$ and $\Delta\varphi_0$, change the Hall resistance R_{Hall}.

To obtain a clear relationship between the SOT fields and R_{Hall}, Eq. (8) can be further simplified. In the absence of an external field acting along z axis ($H_{z\text{-ext}} = 0$), θ_0 can be set to 0, as seen from Eq. (4). From the Pythagorean trigonometric identity and the assumption that $\Delta\theta_0$ and $\Delta\varphi_0$ are small, Eq. (8) is simplified to

$$R_{\text{Hall}} = R_{\text{AHE}}\Delta\theta_0\sin\omega t + R_{\text{PHE}}(\sin 2\varphi_0 + 2\Delta\varphi_0\cos 2\varphi_0)\sin\omega t. \tag{9}$$

According to Eqs. (4)–(7) and using the identity $\sin^2\omega t = \frac{1-\cos 2\omega t}{2}$, Eq. (9) can be rewritten with the SOT induced effective fields being the variables,

$$R_{\text{Hall}} = R_{\text{PHE}}\sin 2\varphi_0\sin\omega t - R_{\text{AHE}}\frac{H_D}{2H_\perp}X\cos 2\omega t - R_{\text{PHE}}\frac{H_F}{H_{x\text{-ext}}}(2X^4 - X^2)\cos 2\omega t + C, \tag{10}$$

where $X = \cos\varphi_0$, and C is a constant. The SOT effective fields H_D and H_F contribute only to the second harmonic Hall resistance amplitude, which is given by

$$R_{2\text{ndHall}} = R_{\text{AHE}}\frac{H_D}{2H_\perp}X + R_{\text{PHE}}\frac{H_F}{H_{x\text{-ext}}}(2X^4 - X^2). \tag{11}$$

Experimentally, H_D and H_F can be extracted from Eq. (11) by keeping $H_{x\text{-ext}}$ constant and varying X by sweeping $H_{y\text{-ext}}$. When $H_{x\text{-ext}}$ is fixed, the coefficient $R_{\text{PHE}}\frac{H_F}{H_{x\text{-ext}}}$ of Eq. (11) is constant. By sweeping the transverse field $H_{y\text{-ext}}$, X becomes the only variable and can be calculated through Eq. (5). The value of X can also be validated by the first harmonic Hall resistance measurement $R_{1\text{stHall}} = R_{\text{PHE}}\sin 2\varphi_0$. Rewriting the expression of $R_{2\text{ndHall}}$, $R_{2\text{ndHall}} = aX + b(2X^4 - X^2)$ and fitting the measured $R_{2\text{ndHall}}$ with respect to the measured X by the above expression, the coefficients, a and b, can be computed. Thus H_D and H_F can be calculated from the values of a and b as

$$H_D = \frac{2H_\perp}{R_{\text{AHE}}}a \quad \text{and } H_F = \frac{H_{x\text{-ext}}}{R_{\text{PHE}}}b. \tag{12}$$

In Eq. (11), the amplitude of planar Hall resistance R_{PHE} can be directly extracted from the first harmonic Hall resistance $R_{1\text{stHall}}$, while $\frac{H_\perp}{R_{\text{AHE}}}$ can be obtained through measuring the anomalous Hall effect. From the expression of AHE and Eq. (4), when the system is magnetically saturated along the normal direction of the film plane, $\sin\theta$ is equal to 1, which results in $\frac{H_{z\text{-ext}}}{H_\perp} = 1$. Thus $\frac{H_\perp}{R_{\text{AHE}}} = \frac{H_{z\text{-ext,satur}}}{R_{\text{AHE}}}$, where $H_{z\text{-ext,satur}}$ is the out-of-plane saturation field.

III. EXPERIMENTAL VERIFICATION

A. Characterization of SOT fields in Ta(6 nm)/Co(2 nm)/Pt(5 nm)

To validate the proposed technique to obtain SOT effective fields using a single measurement, structured samples with IMA were fabricated. A Ta(6 nm)/Co(2 nm)/Pt(5 nm) thin film stack was deposited using DC magnetron sputtering deposition technique. The film stack was patterned into 5-μm-wide wires, using a combination of electron beam lithography (EBL) and Ar+ ion milling techniques. Two 20-μm-wide Hall bars, consisting of Ta(10 nm)/Cu(100 nm)/Ta(10 nm), were deposited on top of the wire by magnetron sputtering, after being patterned by EBL and following liftoff process.

To confirm the in-plane magnetic anisotropy of the film and structure, longitudinal magneto-optic Kerr effect (MOKE) magnetometry and AHE measurements were performed.

The inset of Fig. 1(a) shows the measured longitudinal MOKE loop of the film Ta(6 nm)/Co(2 nm)/Pt(5 nm). The MOKE loop indicates an in-plane magnetization with a switching field of around 20 Oe. The measured AHE resistance, with respect to the out-of-plane field, is shown in Fig. 1(b). From $R_A = R_{AHE}\sin\theta = R_{AHE}\frac{H_{z\text{-ext}}}{H_\perp}$, for the stack Ta(6 nm)/Co(2 nm)/Pt(5 nm), the magnetic moments rotate from in plane at $H_{z\text{-ext}} = 0$ Oe to out of plane at $H_{z\text{-ext}} = 5180$ Oe. Thus, the effective anisotropy field of the wire is $H_\perp = 5180$ Oe.

The first and second harmonic Hall resistances for extracting the SOT effective fields were measured simultaneously using a single 7265 DSP lock-in amplifier connected across the Hall bars. A constant longitudinal field of $H_{x\text{-ext}} = 500$ Oe is applied along the wire direction to ensure uniform magnetization along the FM wire long axis, while a transverse field of $H_{y\text{-ext}}$ is swept from -2000 Oe to $+2000$ Oe. An ac with frequency 307.1 Hz and current density amplitudes ranging from 3×10^{10} Am^{-2} to 1×10^{11} Am^{-2} in steps of 1×10^{10} Am^{-2} were applied across the FM wire. By taking the ratio of the Hall voltages over the amplitudes of the ac, the first and second harmonic Hall resistances can be obtained.

The dependence of the harmonic Hall resistances on the azimuthal angle φ_0, cosine X and constant field $H_{x\text{-ext}}$, are studied. The Hall resistances measured at the current density of 1×10^{11} Am^{-2}, are shown in Fig. 2. The angle φ_0 is calculated simultaneously by Eq. (5), $\tan\varphi_0 = \frac{H_{y\text{-ext}}}{H_{x\text{-ext}}}$, while the transverse field $H_{y\text{-ext}}$ is swept. From Fig. 2(a), we note that the first harmonic Hall resistance $R_{1\text{stHall}}$ measured with a fixed field $H_{x\text{-ext}} = +500$ Oe shows a typical sinusoidal trend with respect to the azimuthal angle of φ_0. For $H_{x\text{-ext}} = -500$ Oe, where the angle sweeps from $+\varphi_0$ to $-\varphi_0$, a similar trend is observed. By fitting the curves with the expression of $R_{1\text{stHall}} = R_{PHE}\sin 2\varphi_0$, we obtain $R_{PHE} = 5.1$ mΩ. The corresponding second harmonic Hall resistances are shown in Fig. 2(b). For $H_{x\text{-ext}} = +500$ Oe, the resistance increases with increasing X. This is consistent with the prediction of Eq. (11) $R_{2\text{ndHall}} = R_{AHE}\frac{H_D}{2H_\perp}X + R_{PHE}\frac{H_F}{H_{x\text{-ext}}}(2X^4 - X^2)$. The expression for the dampinglike term is $\mathbf{H}_D = H_D\mathbf{m}\times\mathbf{s}$. By reversing the direction of magnetization $\mathbf{m}$, the sign of X should also change. To verify this, we measured the resistance $R_{2\text{ndHall}}$ at $H_{x\text{-ext}} = -500$ Oe as shown in Fig. 2(b). The resistance is symmetric with respect to the zero resistance axis, as compared to the $R_{2\text{ndHall}}$ at $H_{x\text{-ext}} = +500$ Oe. This is consistent with the prediction of the expression of $R_{2\text{ndHall}}$. The term $R_{PHE}\frac{H_F}{H_{x\text{-ext}}}(2X^4 - X^2)$ becomes negative with the negative sign of $H_{x\text{-ext}}$, as the sign of H_F is independent of the direction of $\mathbf{m}$. The AHE component $R_{AHE}\frac{H_D}{2H_\perp}X$ becomes negative as well, since the sign of X changes when the direction of magnetization is changed. Thus, $R_{2\text{ndHall}}$ at $-H_{x\text{-ext}}$ is symmetric with $R_{2\text{ndHall}}$ at $+H_{x\text{-ext}}$. In summary, the SOT effective fields, H_F and H_D, guarantee the existence of these dependencies.

Through fitting the second harmonic Hall resistances with the cosine of azimuthal angle X with Eq. (11), the SOT effective fields are calculated for each applied current density in the wire. Figure 3 shows the second harmonic Hall resistances as the current density is varied from 3×10^{10} Am^{-2} to 1×10^{11} Am^{-2}. The resistance with respect to X exhibits

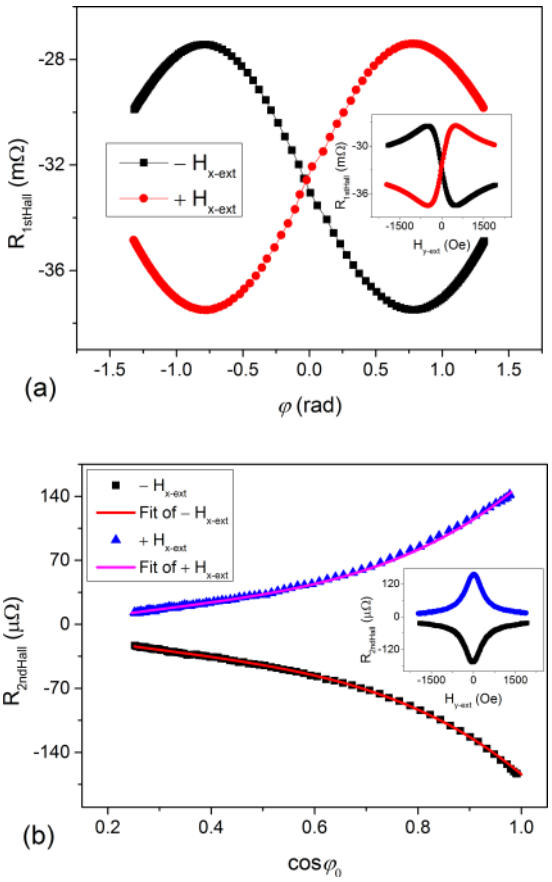

FIG. 2. The first harmonic Hall resistances (a) and the second harmonic Hall resistances (b) under two constant fields $H_{x\text{-ext}}$ with opposite directions. The applied current density is 1×10^{11} Am^{-2}. For (a), both curves show sine function with respect to the azimuthal angle of magnetization; the inset shows the resistance with the external fields $H_{y\text{-ext}}$, which corresponds to the angle. For (b), the resistance at $+H_{x\text{-ext}}$ is approximately symmetric to that at $-H_{x\text{-ext}}$ about 0 Ohm; the inset represents the second harmonic Hall resistance with respect to the external field $H_{y\text{-ext}}$ which corresponds to the cosine of azimuthal angle. The solid line is a fit to the experimental data.

similar dependencies as in Fig. 2(b), where the current density is 1×10^{11} Am^{-2}. Hence the SOT effective fields contribute to the dependencies for each case of current density, 3×10^{10} Am^{-2} to 1×10^{11} Am^{-2}. The absolute values of these resistances increase with increasing current density. $R_{2\text{ndHall}}$ increases from $\sim 40\,\mu\Omega$ at 3×10^{10} Am^{-2} to $\sim 140\,\mu\Omega$ at 1×10^{11} Am^{-2}, when $H_{x\text{-ext}}$ is aligned along the $-x$ direction and $X = 1$. Comparing the experimental result of $R_{2\text{ndHall}}$ with its analytical expression of Eq. (11), $R_{2\text{ndHall}} = R_{AHE}\frac{H_D}{2H_\perp}X + R_{PHE}\frac{H_F}{H_{x\text{-ext}}}(2X^4 - X^2)$, we conclude that this increasing trend represents the increase of H_D or H_F with respect to current densities. For the sample, Ta(6 nm)/Co(2 nm)/Pt(5 nm), R_{AHE} is 24.4 mΩ and $H_\perp$ is 5180 Oe [Fig. 1(b)], R_{PHE} equals to 5.1 mΩ, and $H_{x\text{-ext}}$ is ± 500 Oe. Taking these parameters into Eq. (11) to fit the curves in Figs. 2(b) and 3, H_F and H_D are calculated. Figure 4(a) shows the calculated H_F. The fieldlike term increases from ~ 2 Oe at 3×10^{10} Am^{-2} to ~ 7 Oe at 1×10^{11} Am^{-2}, giving a ratio of H_F to current density of 7 Oe per 10^{11} Am^{-2}. The

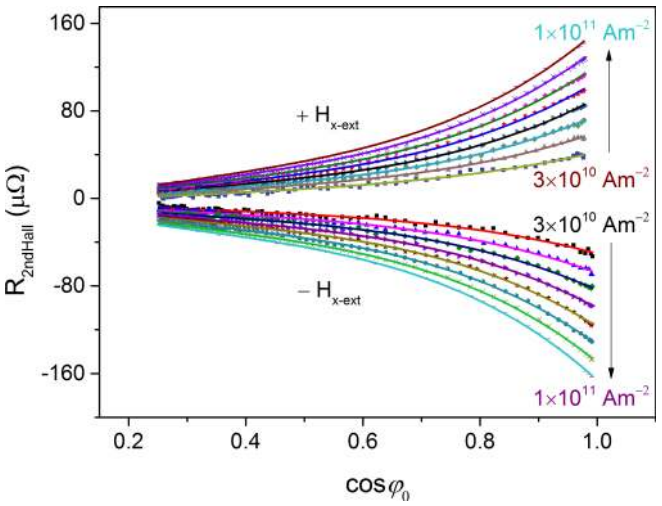

FIG. 3. The second harmonic Hall resistances under two constant fields $H_{x\text{-ext}}$ with opposite directions and different current densities. The current density starts from 3×10^{10} to 1×10^{11} Am^{-2} with a step size 1×10^{10} Am^{-2}. The solid line is a fit to the experimental data.

sign of H_F does not change to negative when the longitudinal $H_{x\text{-ext}}$ is reversed, which is consistent with the expression of $\mathbf{H}_F = H_F\mathbf{s}$. Figure 4(b) shows the calculated H_D. The absolute value of the dampinglike term increases from ~14 Oe at 3×10^{10} Am^{-2} to ~45 Oe at 1×10^{11} Am^{-2}. The ratio of H_D to current density is 44 Oe per 10^{11} Am^{-2}. H_D becomes negative when the longitudinal field $H_{x\text{-ext}}$ is reversed. This is consistent with the expression of $\mathbf{H}_D = H_D\mathbf{m} \times \mathbf{s}$.

B. Dependence of SOT fields on the thickness of Tantalum

To study the dependence of SOT fields on the thickness of Ta, the measurements were repeated in Ta(t_{Ta}nm)/Co(2 nm)/Pt(5 nm), where $t_{Ta} = 2, 4, 8$, and 10. The IMA property of all the samples are confirmed by measurement of AHE and longitudinal MOKE, as shown in Fig. 5(a). R_{AHE} and $H_\perp$ are obtained by measuring AHE as shown in the table of Fig. 5(a). Similar experimental conditions as for Ta(6 nm)/Co(2 nm)/Pt(5 nm) were used to quantify the SOT effective fields. In Fig. 5(a), the harmonic Hall resistances measured at 1×10^{11} Am^{-2} are presented for the three samples investigated. The second harmonic Hall resistances $R_{2ndHall}$ increase with increasing X. For each of the samples, the first harmonic Hall resistances show the typical sinusoidal trend with respect to the azimuthal angle of φ_0. The R_{PHE} values, as shown in the table of Fig. 5(b), can be extracted from the inset of Fig. 5(b). The first and second harmonic Hall resistances of the three samples present the similar behavior as predicted by the expression of $R_{1stHall}$ and $R_{2ndHall}$, hence, the SOT effective fields can be extracted by the proposed method.

The SOT effective fields are characterized in the four samples with different thicknesses of Ta. Figure 6 shows the SOT effective fields for each of the samples. For comparison, the SOT effective fields of Ta(6 nm)/Co(2 nm)/Pt(5 nm) are included. Both H_F [Fig. 6(a)] and H_D [Fig. 6(b)] show general increasing trends with respect to the thickness for all current densities. The trends are consistent with that reported

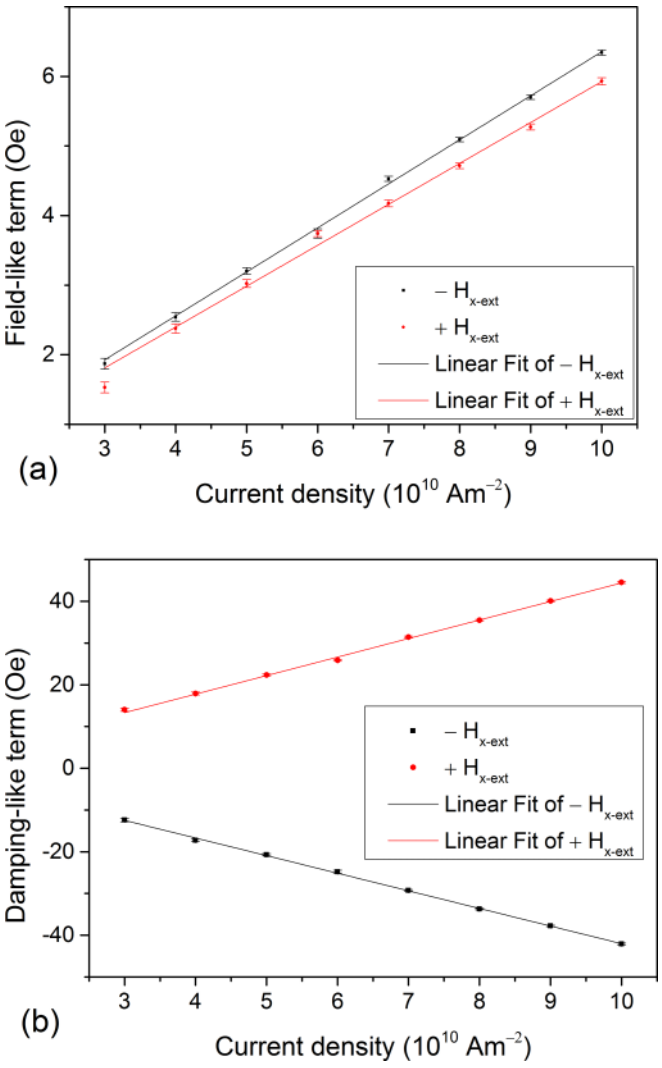

FIG. 4. Amplitudes of fieldlike term (a) and dampinglike term (b) with respect to the applied current density. The dampinglike term changes its sign when $H_{x\text{-ext}}$ is reversed whereas the fieldlike term does not change its direction. The slopes of fieldlike term and dampinglike term over the current density are ~7 Oe per 10^{11} Am^{-2} and ~44 Oe per 10^{11} Am^{-2}. The error bars indicate the uncertainty in fitting the Eq. (11).

in stacks with PMA [10,18,36]. It is proposed that the amount of current flowing in the Ta layer increases as t_{Ta} is increased, as such, the SOT effective fields increase with t_{Ta}. This point is also applicable in our case, as the resistance of the patterned wires reduces with increasing the thickness of Ta as shown in Fig. 7. However, from the sample with 8 nm to that with 10 nm, H_F keeps approximately constant, while H_D shows significant increases, compared to the H_D values with thinner Ta thickness. H_F at the current density of 1×10^{11} Am^{-2}, for instance, keeps ~6.7 Oe; while the change rate of H_F to t_{Ta} is ~4 Oe nm^{-1} for $t_{Ta} = 6$ and 8, increases to ~11 Oe nm^{-1} for $t_{Ta} = 8$ and 10. This abnormal behavior is likely due to the dependence of SOT fields on the saturation magnetization of Co layers. As shown in the inset of Fig. 6(b), the saturation magnetization exhibits a significant increase from $t_{Ta} = 8$ to $t_{Ta} = 10$. This implies the dampinglike term increases while

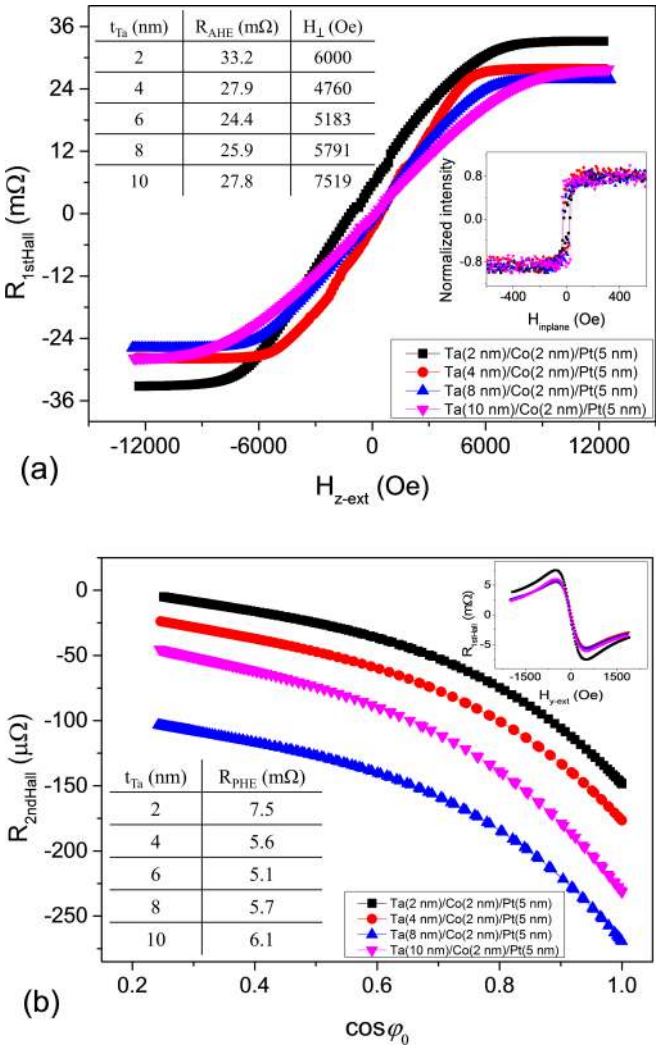

FIG. 5. (a) Resistance of AHE and normalized longitudinal MOKE loop (inset). (b) The fitted second harmonic resistances with respect to the azimuthal angle of magnetization for different stacks, the inset is the first harmonic resistance with respect to the applied transverse field; the sets of curves show similar characterization to those in Figs. 3(a) and 3(b), respectively, for the thin films with different stacks.

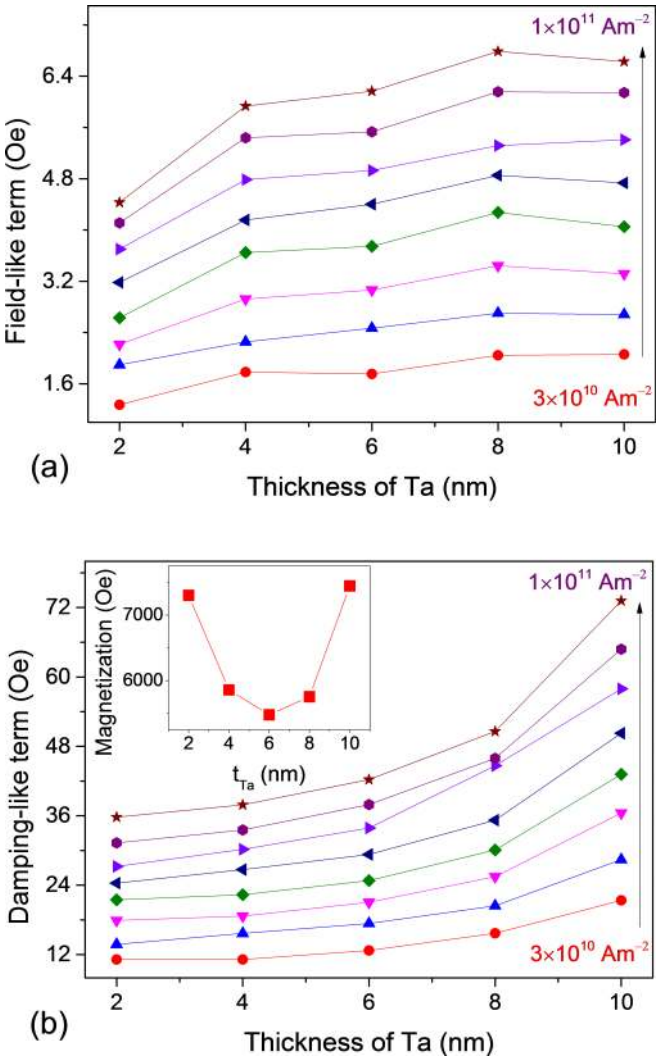

FIG. 6. Amplitudes of fieldlike term (a) and dampinglike term (b) with respect to the thickness of Ta for different current densities.

the fieldlike term decreases with respect to the magnetization of Co layers. The behaviors can also be observed in samples with $t_{\mathrm{Ta}} = 2, 4$, and 6. A larger decrease in magnetization is found from $t_{\mathrm{Ta}} = 2$ to 4 compared to the decrease from $t_{\mathrm{Ta}} = 4$ to 6. As such, in addition to the influence from the thickness dependence, the increase in H_F for $t_{\mathrm{Ta}} = 2$ to 4 is more significant than $t_{\mathrm{Ta}} = 4$ to 6, while H_D shows insignificant increase. The magnetization dependence is consistent with the expectation that the SOT effective fields are likely related to the efficiency of spin diffusion across the Ta/Co interface instead of an intrinsic property [23,36], as the asymmetric spin scattering can be enhanced by increasing the magnetization of magnetic film [52]. In conclusion, the dependence of the effective SOT fields is ascribed to the increasing of current flowing in the Ta layer and the change of efficiency of spin diffusion across the Ta/Co interface.

The effective spin Hall angles are calculated to enable comparison with other methodologies. The spin Hall angle, θ_{SH}, in our film stack is computed by using the following expression as $\theta_{SH} = \frac{2eM_s t_F}{\hbar}\frac{H_D}{j}$ [9,17,42,43], where e is the

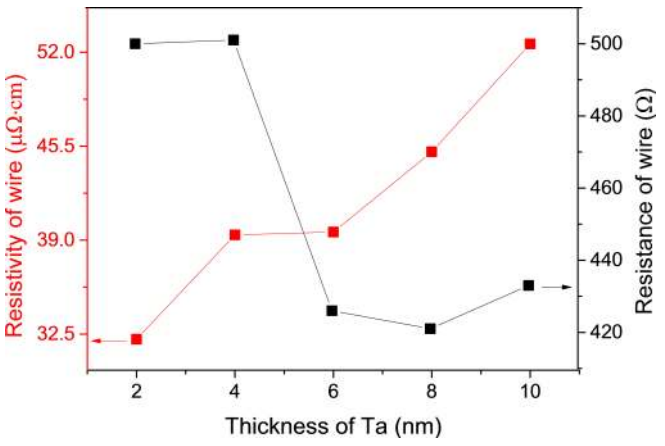

FIG. 7. The resistance and corresponding resistivity of patterned wires with different Ta film thicknesses.

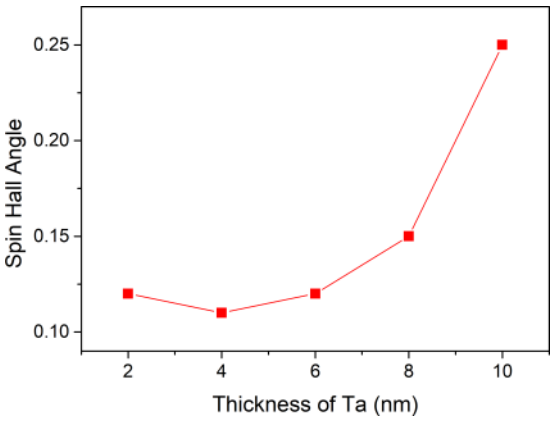

FIG. 8. The computed effective spin Hall angles of the Ta/Co/Pt stacks as a function of Ta film thicknesses.

electron charge, $\hbar$ is the reduced Planck constant, and t_F is the thickness of Co layer. The calculated θ_{SH} in our film stack, as a function of Ta film thicknesses is plotted in Fig. 8. For Ta thickness of $t_{\mathrm{Ta}} \leqslant 6\,\mathrm{nm}$, θ_{SH} is computed to ~0.11. As the bottom Ta layer in our film stack was used as a seed layer, the interaction with SiO_2 on the substrate leads to the oxidation of the first few layers of Ta at the interface [53,54]. As such, for small Ta thicknesses, the spin Hall effect is mainly due to the Pt layer. The θ_{SH} of Pt has been reported to be ~0.07 as measured by ST-FMR [35], 0.06 ± 0.02 as measured by SOT induced magnetization switching [22], and 0.06 as measured by current induced domain-wall motion [8]. For $t_{\mathrm{Ta}} > 6\,\mathrm{nm}$, θ_{SH} increases from 0.15, reaching a maximum of 0.25 for $t_{\mathrm{Ta}} = 10\,\mathrm{nm}$. This is attributed to the contribution of SOT from the Ta film. The percentage of the β-phase Ta, which has been reported to have a large θ_{SH}, increases with the thickness of Ta [23,35,36]. Additionally, the growth of Ta on SiO_2 has been reported to promote the Ta β phase [55,56]. To ascertain the presence of β-phase Ta in our film stack, the resistance of the film stack was monitored as described by Ref. [23]. As shown in Fig. 7, the wire resistance does not reduce significantly with increasing t_{Ta}, which suggests that the fraction of β-phase Ta increases in the film stacks [23]. The increase of wire resistivity further confirms that the fraction of β phase increases, as it is known to have a higher resistivity. The largest spin Hall angle in our film stack is 0.25 and was obtained in the stack comprising of Ta(10 nm)/Co(2 nm)/Pt(5 nm). Considering that effective spin Hall angle is equal to individual contribution from both Ta and Pt, the spin Hall angle of Ta is calculated to be (0.25–0.07 =)0.18, where θ_{SH} of Pt is chosen as ~0.07. This value is consistent with the reported value ~0.12 as measured by ST-FMR [35,36]. For the stack of Ta(8 nm)/Co(2 nm)/Pt(5 nm), the effective spin Hall angle is ~0.15, and the spin Hall angle contribution of Ta is calculated to be 0.08. This value is larger than ~0.025 as measured by harmonic Hall voltage technique [57], ~0.02 measured by ST-FMR [41]. The two different values of spin Hall angle for Ta as measured in our film stacks suggest that the percentage of β-phase Ta can be a contributing factor in different spin Hall angles of Ta.

IV. CONCLUSION

An analytical expression to obtain both the fieldlike and dampinglike effective fields in IMA structure is derived. Based on the derived expression, a single harmonic Hall measurement is sufficient to quantify both the fieldlike and dampinglike terms, bypassing different experimental conditions using a two measurement scheme that usually leads to artefacts. SOT harmonic Hall measurements in IMA structure were performed and our analytical derivations are used to extract the SOT fields. The dependence of SOT strength on the Ta thickness was also investigated in the IMA structure, where the fieldlike term and dampinglike terms were determined concurrently. In conclusion, our proposed measurement method paves the way for consistent quantifications of the SOT effective fields in IMA structure.

ACKNOWLEDGMENTS

This work was supported by the Singapore National Research Foundation, Prime Minister's Office, under a Competitive Research Programme (Non-volatile Magnetic Logic and Memory Integrated Circuit Devices, NRF-CRP9-2011-01), and an Industry-IHL Partnership Program (NRF2015-IIP001-001). The work was also supported by a MOE-AcRF Tier 2 Grant (MOE 2013-T2-2-017). W.S.L. is a member of the Singapore Spintronics Consortium (SG-SPIN).

[1] A. Manchon and S. Zhang, Phys. Rev. B **78**, 212405 (2008); **79**, 094422 (2009).
[2] E. I. Rashba, Sov. Phys. Solid State **2**, 1224 (1960).
[3] M. I. Dyakonov and V. I. Perel, Phys. Lett. A **35**, 459 (1971).
[4] Y. A. Bychkov and E. I. Rashba, J. Phys. C **17**, 6039 (1984).
[5] J. Stohr and H.C. Siegmann, *Magnetism from Fundamentals to Nanoscale Dynamics* (Springer-Verlag, Berlin, Heidelberg, 2006), p. 107.
[6] I. M. Miron, G. Gaudin, S. Auffret, B. Rodmacq, A. Schuhl, S. Pizzini, J. Vogel, and P. Gambardella, Nat. Mater. **9**, 230 (2010).
[7] I. M. Miron, K. Garello, G. Gaudin, P.-J. Zermatten, M. V. Costache, S. Auffret, S. Bandiera, B. Rodmacq, A. Schuhl, and P. Gambardella, Nature (London) **476**, 189 (2011).
[8] S. Emori, U. Bauer, S.-M. Ahn, E. Martinez, and G. S. D. Beach, Nat. Mater. **12**, 611 (2013).
[9] X. Fan, H. Celik, J. Wu, C. Ni, K.-J. Lee, V. O. Lorenz, and J. Q. Xiao, Nat. Commun. **5**, 3042 (2014).
[10] T. D. Skinner, K. Olejník, L. K. Cunningham, H. Kurebayashi, R. P. Campion, B. L. Gallagher, T. Jungwirth, and A. J. Ferguson, Nat. Commun. **6**, 6730 (2015).
[11] L. Berger, Phys. Rev. B **54**, 9353 (1996).
[12] J. C. Slonczewski, J. Magn. Magn. Mater. **159**, L1 (1996); **247**, 324 (2002).
[13] S. Zhang, P. M. Levy, and A. Fert, Phys. Rev. Lett. **88**, 236601 (2002).
[14] S. Zhang and Z. Li, Phys. Rev. Lett. **93**, 127204 (2004).

[15] K. Garello, I. M. Miron, C. O. Avci, F. Freimuth, Y. Mokrousov, S. Blügel, S. Auffret, O. Boulle, G. Gaudin, and P. Gambardella, Nat. Nanotechnol. **8**, 587 (2013).
[16] X. Wang and A. Manchon, Phys. Rev. Lett. **108**, 117201 (2012).
[17] S.-M. Seo, K.-W. Kim, J. Ryu, H.-W. Lee, and K.-J. Lee, Appl. Phys. Lett. **101**, 022405 (2012).
[18] J. Kim, J. Sinha, M. Hayashi, M. Yamanouchi, S. Fukami, T. Suzuki, S. Mitani, and H. Ohno, Nat. Mater. **12**, 240 (2013).
[19] M. Jamali, K. Narayanapillai, X. Qiu, L. M. Loong, A. Manchon, and H. Yang, Phys. Rev. Lett. **111**, 246602 (2013).
[20] M. Hayashi, J. Kim, M. Yamanouchi, and H. Ohno, Phys. Rev. B **89**, 144425 (2014).
[21] S. Emori, D. C. Bono, and G. S. D. Beach, Appl. Phys. Lett. **101**, 042405 (2012).
[22] L. Q. Liu, O. J. Lee, T. J. Gudmundsen, D. C. Ralph, and R. A. Buhrman, Phys. Rev. Lett. **109**, 096602 (2012).
[23] S. Woo, M. Mann, A. J. Tan, L. Caretta, and G. S. D. Beach, Appl. Phys. Lett. **105**, 212404 (2014).
[24] H. R. Lee, K. Lee, J. Cho, Y. H. Choi, C. Y. You, M. H. Jung, F. Bonell, Y. Shiota, S. Miwa, and Y. Suzuki, Sci. Rep. **4**, 6548 (2014).
[25] X. Qiu, P. Deorani, K. Narayanapillai, K.-S. Lee, K.-J. Lee, H.-W. Lee, and H. Yang, Sci. Rep. **4**, 4491 (2014).
[26] M. Montazeri, P. Upadhyaya, M. C. Onbasli, G. Yu, K. L. Wong, M. Lang, Y. Fan, X. Li, P. K. Amiri, R. N. Schwartz, C. A. Ross, and K. L. Wang, Nat. Commun. **6**, 8958 (2015).
[27] X. Qiu, K. Narayanapillai, Y. Wu, P. Deorani, D. H. Yang, W. S. Noh, J. H. Park, K. J. Lee, H. W. Lee, and H. Yang, Nat. Nanotechnol. **10**, 333 (2015).
[28] D. Chiba, M. Kawaguchi, S. Fukami, N. Ishiwata, K. Shimamura, K. Kobayashi, and T. Ono, Nat. Commun. **3**, 888 (2012).
[29] P. P. J. Haazen, E. Mure, J. H. Franken, R. Lavrijsen, H. J. M. Swagten, and B. Koopmans, Nat. Mater. **12**, 299 (2013).
[30] K. S. Ryu, L. Thomas, S. H. Yang, and S. Parkin, Nat. Nanotechnol. **8**, 527 (2013).
[31] T. Kimura, Y. Otani, T. Sato, S. Takahashi, and S. Maekawa, Phys. Rev. Lett. **98**, 156601 (2007).
[32] K. Ando, S. Takahashi, K. Harii, K. Sasage, J. Ieda, S. Maekawa, and E. Saitoh, Phys. Rev. Lett. **101**, 036601 (2008).
[33] O. Mosendz, J. E. Pearson, F. Y. Fradin, G. E. W. Bauer, S. D. Bader, and A. Hoffmann, Phys. Rev. Lett. **104**, 046601 (2010).
[34] L. Liu, T. Moriyama, D. C. Ralph, and R. A. Buhrman, Phys. Rev. Lett. **106**, 036601 (2011).
[35] L. Liu, C. F Pai, Y. Li, H. W. Tseng, D. C. Ralph, and R. A. Buhrman, Science **336**, 6081 (2012).
[36] G. Allen, S. Manipatruni, D. E. Nikonov, M. Doczy, and I. A. Young, Phys. Rev. B **91**, 144412 (2015).
[37] K. Ueda, C. F. Pai, A. J. Tan, M. Mann, and G. S. D. Beach, Appl. Phys. Lett. **108**, 232405 (2016).
[38] X. Qiu, W. Legrand, P. He, Y. Wu, J. Yu, R. Ramaswamy, A. Manchon, and H. Yang, Phys. Rev. Lett. **117**, 217206 (2016).
[39] T. Suzuki1, S. Fukami, N. Ishiwata, M. Yamanouchi, S. Ikeda, N. Kasai, and H. Ohno, Appl. Phys. Lett. **98**, 142505 (2011).
[40] M. Morota, Y. Niimi, K. Ohnishi, D. H. Wei, T. Tanaka, H. Kontani, T. Kimura, and Y. Otani, Phys. Rev. B **83**, 174405 (2011).
[41] C. Hahn, G. de Loubens, O. Klein, M. Viret, V. V. Naletov, and J. Ben Youssef, Phys. Rev. B **87**, 174417 (2013).
[42] A. V. Khvalkovskiy, V. Cros, D. Apalkov, V. Nikitin, M. Krounbi, K. A. Zvezdin, A. Anane, J. Grollier, and A. Fert, Phys. Rev. B **87**, 020402 (2013).
[43] S. Fukami, T. Anekawa, C. Zhang, and H. Ohno, Nat. Nanotechnol. **11**, 621 (2016).
[44] U. H. Pi, K. W. Kim, J. Y. Bae, S. C. Lee, Y. J. Cho, K. S. Kim, and S. Seo, Appl. Phys. Lett. **97**, 162507 (2010).
[45] A. R. Mellnik, J. S. Lee, A. Richardella, J. L. Grab, P. J. Mintun, M. H. Fischer, A. Vaezi, A. Manchon, E.-A. Kim, N. Samarth, and D. C. Ralph, Nature **511**, 449 (2014).
[46] Y. Fan, P. Upadhyaya, X. Kou, M. Lang, S. Takei, Z. Wang, J. Tang, L. He, L.-T. Chang, M. Montazeri, G. Yu, W. Jiang, T. Nie, R. N. Schwartz, Y. Tserkovnyak, and K. L. Wang, Nat. Mater. **13**, 699 (2014).
[47] Y. Wang, P. Deorani, K. Banerjee, N. Koirala, M. Brahlek, S. Oh, and H. Yang, Phys. Rev. Lett. **114**, 257202 (2015).
[48] S. Chikazumi, and C. D. Graham, *Physics of Ferromagnetism*, 2nd ed. (Oxford University Press, 2009), Chap. 18, p. 472.
[49] H. Sato, M. Yamanouchi, K. Miura, S. Ikeda, R. Koizumi, F. Matsukura, and H. Ohno, IEEE Magn. Lett. **3**, 3000204 (2012).
[50] T. R. McGuire and R. I. Potter, IEEE Trans. Magn. **11**, 1018 (1975).
[51] H. X. Tang, R. K. Kawakami, D. D. Awschalom, and M. L. Roukes, Phys. Rev. Lett. **90**, 107201 (2003).
[52] V. V. Ustinov, Zh. Eksp. Teor. Fiz. **106**, 207 (1994).
[53] P. Gallais, J. J. Hantzpergue, and J. C. Remy, Thin Solid Films **165**, 227 (1988).
[54] S. Rogojevic, A. Jain, F. Wang, W. N. Gill, P. C. Wayner, Jr., J. L. Plawsky, T.-M. Lu, G.-R. Yang, W. A. Lanford, A. Kumar, H. Bakhru, and A. N. Roy, J. Vac. Sci. Technol. B **19**, 354 (2001).
[55] H. J. Zhang, S. Yamamoto, Y. Fukaya, M. Maekawa, H. Li, A. Kawasuso, T. Seki, E. Saitoh, and K. Takanashi, Sci. Rep. **4**, 4844 (2014).
[56] J. J. Senkevich, T. Karabacak, D.-L. Bae, and T. S. Cale, J. Vac. Sci. Technol. B **24**, 534 (2006).
[57] C. Zhang, M. Yamanouchi, H. Sato, S. Fukami, S. Ikeda1, F. Matsukura, and H. Ohno, Appl. Phys. Lett. **103**, 262407 (2013).